Hydrodynamics of Slug Flow Applied to Cross-Flow Filtration in Narrow Tubes

Muriel Mercier-Bonin, Claude Maranges, Christine Lafforgue, and Christian Fonade
Institut National des Sciences Appliquées, Laboratoire de Biotechnologie-Bioprocédés UMR CNRS 5504, LA INRA, 135 Avenue de Rangueil, 31077 Toulouse cedex 4, France

Alain Line
Institut National des Sciences Appliquées, Laboratoire d'Ingénierie et Procédés de l'Environnement, 135 Avenue de Rangueil, 31077, Toulouse cedex 4, France

This article focuses on the characterization of slug-flow hydrodynamics in two sizes of tubular membrane diameters (6 and 15 mm) to quantify the main mechanical phenomena involved in the limitation of particle fouling during cross-flow filtration of suspensions. By using a conductance probe technique, the flow structure was accurately identified for two geometries, and noticeable differences were observed in terms of void fractions, velocities and lengths of Taylor bubbles, and liquid slugs. This characterization allowed some data to be theoretically estimated (wall shear stress, ''falling'' film velocity, film thickness) thanks to the application of a phenomenological model initially developed for oil pipes. The results obtained in a 15-mm tube showed that the ultrafiltration flux improvement, experimentally achieved with bentonite and yeast suspensions, was partly due to the increase in the wall shear stress, induced by continuous gas sparging inside the tubular filtration module. Other hydrodynamic phenomena linked to the quasi-periodic succession of Taylor bubbles and liquid slugs were also involved in the control of the particle entrainment: intermittency frequency, reversal of the wall shear stress, instantaneous pressure variations in the long bubble wake with a higher level of turbulence, and an enhanced local mixing.

Introduction

Cross-flow filtration is a very useful downstream process in the food and biochemical industries for concentration, purification, and separation of macromolecules, colloids, and suspended particles from solutions. Membrane separation is also considered to be one of the most promising single operations that can be coupled with continuous fermentation to maintain high bioconversion yields (Ferras et al., 1986; Bibal et al., 1991). However, as the fluid to be filtered contains many suspended solids and soluble compounds, the decrease in flux that is attributed to membrane fouling limits its industrial development compared to other traditional separation methods. In most cases, the main cause of the flux decline is due to the formation of an external fouling layer on the membrane surface (particle deposit, for instance). For that reason, specific hydrodynamic conditions have been proposed for improving filtration performance by ensuring a continuous mixing of the fluid: turbulence promoters (Finnigan and Howell, 1990), rotating membranes (Kroner et al., 1987), Dean vortices (Moulin et al., 1996), and unsteady flows, such as pulsating flows (Gupta et al., 1992) or intermittent jets (Arroyo and Fonade, 1993; Maranges and Fonade, 1997). Even though these methods often required either specific membranes or network modifications, the efficiency was generally improved compared to conventional steady cross-flow filtration.

The present article deals with another kind of flow modification, which consists of a continuous gas injection inside the filtration module in order to create a two-phase gas/liquid flow with unsteady characteristics, called slug flow. This principle has been successfully applied to several applications, such as biological treatment (Lee et al., 1993; Léonard et al.,

Correspondence concerning this article should be addressed to M. Mercier-Bonin.

1998; Mercier et al., 1998), drinking-water production (Cabassud et al., 1997), and separation of macromolecules (Cui and Wright, 1994, 1996), in different kinds of filtration modules and experimental conditions. Gas sparging has thus proved to be an effective, simple, and low-cost technique for enhancing filtration performance. Several mechanisms involved in this flux enhancement have been identified and qualitatively described for each membrane geometry. For tubular membranes, it was postulated that the two-phase flow generated complex hydrodynamic conditions inside the filtration module that limited the accumulation of particles or molecules by creating local velocity and pressure fluctuations related to intermittency (Mercier et al., 1997). Other workers (Cui and Wright, 1996) pointed out that the bubble-induced secondary flows played a major role by promoting local mixing in the bubble wake. For hollow-fiber membrane systems, physical displacement of the mass-transfer boundary layer (Bellara et al., 1996) and high shear stresses (Cabassud et al., 1997) were thought to be the main reasons for the observed flux improvement.

In order to optimize the process efficiency, it was very important to understand and quantify the details of slug-flow dynamics and to identify their effect on ultrafiltration and microfiltration performance. It is the intent of the work reported here to characterize more accurately the hydrodynamic behavior of slug flow in a vertical tube with no suction. Since the filtration rates are relatively low compared to the main flow velocity (10^{-5}–10^{-4} m·s^{-1} against 1–10 m·s^{-1}), we can indeed consider that the suction due to filtration doesn't have a significant influence on the flow structure (Maranges, 1995). This hydrodynamic study was focused on the two pipe diameters used during previous ultrafiltration experiments (6 and 15 mm) (Mercier et al., 1997, 1998). First, the pressure variations, recorded for a constant mean transmembrane pressure, were analyzed and discussed. The influence of the flow frequency was also evaluated. Second, the hydrodynamic characteristics of slug flow, including void fractions, lengths, and velocities of Taylor bubbles and liquid slugs, were determined by electrical conductance measurements. This experimental procedure was then completed by a phenomenological approach to calculate further information that was not easily accessible by direct experiments (wall shear stress, film velocity, and thickness). All these data were then helpful in correlating the flux improvements due to the two-phase flow structure with the modification of the local hydrodynamics inside the filtration module. In the same way, the influence of the membrane diameter on the slug-flow structure was also investigated in order to identify for each tubular geometry the dominant mechanisms involved in the process efficiency.

Experimental Investigation

Experimental conditions

The experimental setup has been described elsewhere (Mercier et al., 1997). The tubular filters used in the previous experiments were this time replaced by PVC tubes of the same inner diameter (6 and 15 mm) and length (120 cm and 75 cm, respectively). The experiments were carried out in a vertical upward cocurrent air/water system where the gas and liquid phases were supplied separately. Except for the conductance measurements, the mean transmembrane pressure was maintained at 1.1 bar by adjusting the outflow of the retentate by means of a valve located just downstream of the membrane. The ratio between the gas and liquid flow rates determined a slug-flow pattern inside the tube (Figure 1).

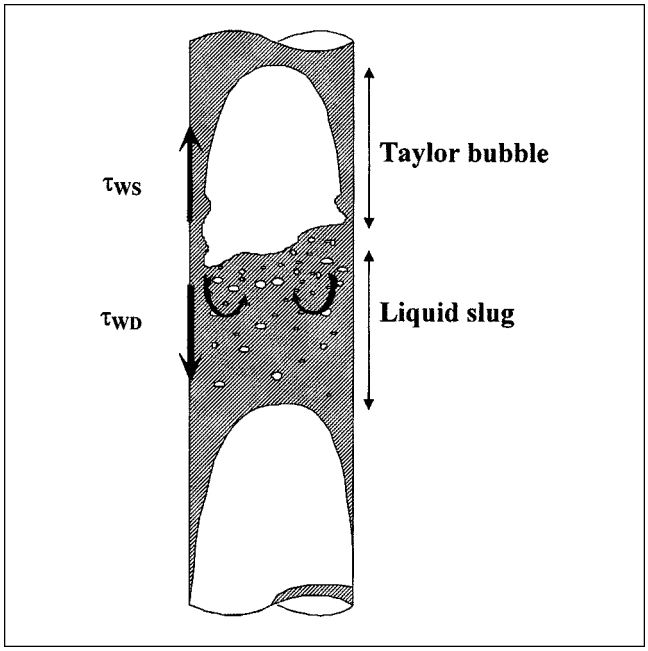

Figure 1. Slug Flow.

For the 15-mm-ID tube, the ranges of flow rates used were $Q_L = 0.14$–0.55 m^3·h^{-1} for the liquid and $Q_G = 0.10$–0.60 m^3·h^{-1} for the gas at the mean pressure of the fluid. The values of the gas flow rate were corrected according to the system pressure because of the gas compressibility. The corresponding superficial velocities, calculated as if each phase was circulating separately, were, respectively, $j_L = 0.22$–0.87 m·s^{-1} and $j_G = 0.16$–0.94 m·s^{-1}. For the 6-mm-ID tube, the experiments were carried out over a wide range of liquid flow rates 0.07–0.29 m^3·h^{-1} ($j_L = 0.69$–2.85 m·s^{-1}) and gas flow rates 0.02–0.47 m^3·h^{-1} ($j_G = 0.20$–4.62 m·s^{-1}). All these flow conditions (transmembrane pressure, liquid and gas flow rates) were chosen on the basis of previous filtration experiments (Mercier et al., 1997, 1998).

Characterization of slug-flow hydrodynamics

Measuring Principle. The first requirement when using an electrical probe in two-phase flow is that the phases have significantly different electrical conductivities, which is the case in an air/water system. Consequently, variations in conductance allow the measurement of the area average void fraction and the arrival frequency of the bubbles at a given point in a continuous, conducting fluid. Statistical information can thus be obtained to characterize the flow pattern.

In this study, the area average void fractions in the Taylor bubbles and in the liquid slugs were measured by processing the signal from conductivity probes made of two stainless-steel ring electrodes mounted at a distance of $3D$ (D = inner diameter of the pipe) to provide adequate spatial resolution for

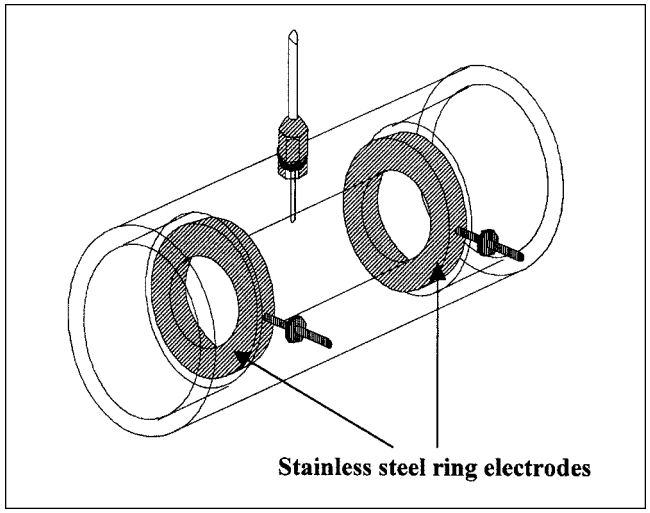

Figure 2. Conductance probe.

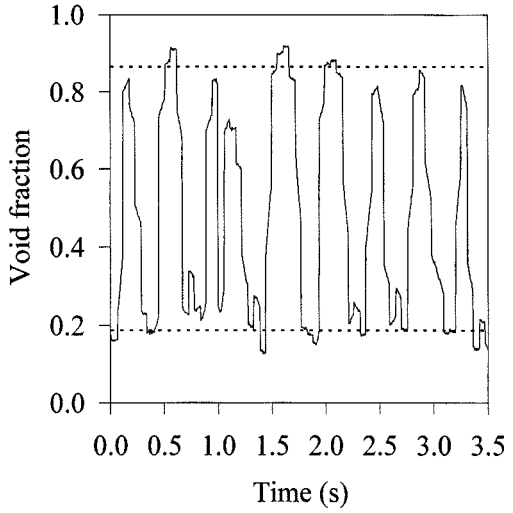

Figure 3. Variation of the void fraction with time for D = 15 mm: $j_L = 0.5\ \mathrm{m \cdot s^{-1}}$; $j_G = 0.7\ \mathrm{m \cdot s^{-1}}$.

the flow conditions under examination (Figure 2). The mean conductivity led directly to the average void fractions using a calibration curve (details are given later). The resolution bandwidth of these probes was high enough to account for the variations of unsteady hydrodynamics. The distance between the injection nozzle and the first probe was sufficient to ensure steady-state conditions within the measuring section. Owing to the stochastic nature of gas/liquid slug flow, a series of 20 measurements was taken for each given pair of gas and liquid flow rates. The conductivity probes were supplied with a 10-kHz electrical current, the frequency of which was significantly different from that of the physical phenomenon to be observed. Impedance changes due to the modification of phase distribution between the two electrodes produced a variation in the output signal that was sampled continuously by a personal computer. In the present investigation, the chosen sampling frequency was 200 Hz. For each single sample, 3500 points were recorded, giving a total duration of 17 s. All the information digitized by the computer was recorded for further processing.

Calibration of the Conductivity Probes. In order to simplify the experimental procedure, the calibration of the conductivity probes was first realized in a static mode, in a horizontal stratified flow pattern. Increasing proportions of liquid phase were injected so that the global average void fraction (R_G) varied from 0% to 100%. The probe was then closed and connected to measure the corresponding voltage. According to several workers (Gadoin, 1993), the calibration of the conductivity probes needs separate measurements of the conductivity of the gas ($U_{\min}$) and the liquid phase ($U_{\max}$). The experimental voltage (U) was then converted by introducing a nondimensional variable u defined as follows:

$$u = \frac{U - U_{\min}}{U_{\max} - U_{\min}}.$$

The result of a regression analysis between R_G and u approximated well to a first-order polynomial law: $R_G = 0.95 - 0.955u$ in the case of a 15-mm-ID tube. A large number of runs was done to check the reliability and the accuracy of the calibration curve. To complete this analysis, another experiment was carried out in a vertical flow pattern with different PVC logs to simulate the gas-phase presence in the core of the tube. The experimental results agreed well with the empirical law previously established. In the case of the 6-mm-ID tube, the calibration results remained the same.

Statistical Analysis. The raw signals obtained for the slug-flow pattern were processed to extract meaningful statistical information. With time the variation of the average void fraction revealed the typical intermittent structure of this flow for both geometries. An example is presented on Figure 3. It was thus possible to distinguish between the large Taylor bubbles, where the void fraction nearly attained a value of unity, and the body of liquid slugs, where the void fraction fluctuated around a much smaller mean value. Such a histogram was used to construct the probability density, which was characterized by a bimodal distribution (Figure 4). The

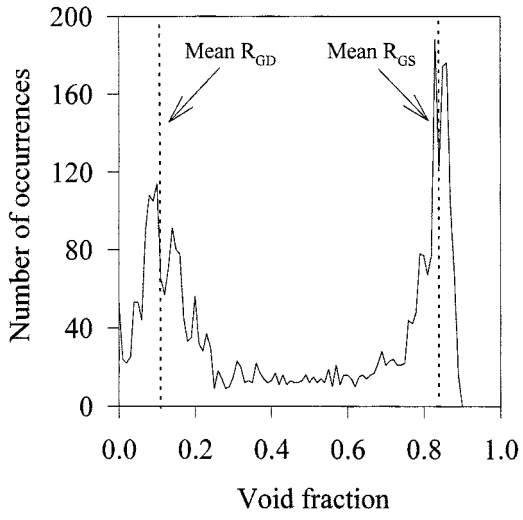

Figure 4. Probability density of void fraction for D = 6 mm: $j_L = 1.2\ \mathrm{m \cdot s^{-1}}$; $j_G = 1.2\ \mathrm{m \cdot s^{-1}}$.

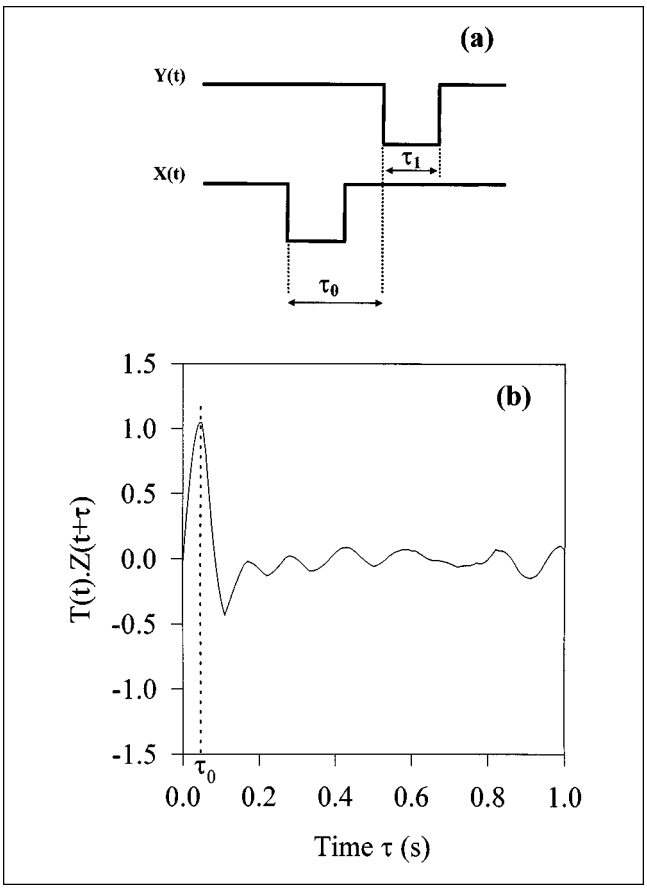

Figure 5. Measurement of bubble velocity for $D = 6$ mm: $j_L = 2.7\ \mathrm{m \cdot s^{-1}}$; $j_G = 0.7\ \mathrm{m \cdot s^{-1}}$.

(a) Principle of measurement; (b) cross-correlation function

$$T(t) = \frac{X(t) - \bar{X}}{|X(t) - \bar{X}|} \quad Z(t) = \frac{Y(t) - \bar{Y}}{|Y(t) - \bar{Y}|},$$

where X and Y are the two probe signals and the overbar represents the mean value of the corresponding data.

two peaks that allowed the precise determination of the mean values of void fraction in the liquid slugs (R_{GD}) and in the long bubbles (R_{GS}) were separated by a deep "valley" region with a low number of occurrences.

The bubble velocity V was determined from the signals of two probes located in series at a distance d of 17 or 74 cm, depending on the flow velocity. A bubble that contacted the first probe would in general subsequently make contact with the second probe. The time delay between these two contact signals was an accurate measure of the velocity of the bubble (Figure 5a). A correlation technique was required to determine the most probable time delay between the two stochastic signals. The cross-correlation function of the two probe signals X and Y is shown in Figure 5b. The maximum of the correlation function yielded the most probable time delay τ_0 from which the bubble velocity was determined as follows: $V = d/\tau_0$. The time between two consecutive Taylor bubbles (τ_1), multiplied by the appropriate translational velocity (V), gave the length of the liquid slugs (Figure 5a). The same procedure was applied to estimate the length of the Taylor bubbles.

Pressure measurements

To examine the variations with time of pressure inside the tube, the experimental conditions (diameter of the tube, liquid and gas flow rates, sampling frequency, duration of measurements) were the same as those for the conductance measurements. For a mean transmembrane pressure of 1.1 bar, the pressure changes were recorded with Validyne pressure transducers DP 15 (range of 0–3 bar, dynamic response of 2×10^{-4} sec) at four different points along the tube in order to detect any spatial perturbation. Probe signals were then processed by the fast Fourier transform using the commercial Easylx software (Keithley) in order to obtain the power spectral density function.

Results and Discussion

Pressure variations in 6- and 15-mm inner diameters

Analysis of Pressure Signals. In 15- and 6-mm-ID tubes, for a given mean transmembrane pressure, the pressure variation with time showed at any point in the flow a nearly periodic signal with instantaneous pressure decreases whose amplitude could reach 0.3 and 0.65 bar for 15-mm- and 6-mm-ID tubes, respectively (Figures 6a and 6b). The amplitude was shown to vary with the mixture velocity j, which is defined as the sum of the superficial velocities of the gas and liquid

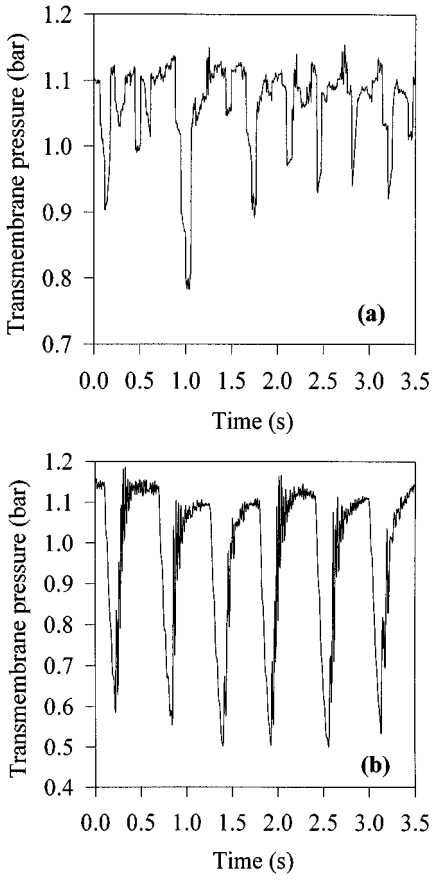

Figure 6. Variation of the transmembrane pressure with time.

(a) $D = 15$ mm ($j_L = 0.5\ \mathrm{m \cdot s^{-1}}$ and $j_G = 0.6\ \mathrm{m \cdot s^{-1}}$); (b) $D = 6$ mm ($j_L = 1.2\ \mathrm{m \cdot s^{-1}}$ and $j_G = 2\ \mathrm{m \cdot s^{-1}}$).

phases ($j = j_L + j_G$). These peaks of low pressure were generated in the wake of rising bubbles, and the phenomenon could easily be explained by the structure of this region, located just behind the Taylor bubbles. These bubbles are in fact followed by liquid slugs containing amounts of small gas bubbles similar in size and motion to those observed in bubbly flow. The small bubbles are distributed almost uniformly over the length of the liquid slug, except for a small region just behind the tail of the preceding Taylor bubble, where the void fraction is considerably higher than that in the bulk of the liquid slug. This locally higher gas fraction is the result of the entrainment of gas from the back of the Taylor bubble by the "falling" liquid film, thereby creating a strong mixing effect and enhancing turbulent activity and mass transfer.

From these observations, we concluded that the local pressure fluctuations of amplitude that varied with respect to experimental conditions (diameter, gas, and liquid flow rates) could easily act on the degree of compaction of the particle deposit and induce a sequential destabilization due to the intermittency of the flow. This phenomenon was surely involved in the overall flux enhancement, as reported by Doubrovine (1992) in the case of an oscillatory flow. In the same way, Maranges and Fonade (1997) using an intermittent jet have shown that hydrodynamic mechanisms linked to pressure variations inside the membrane could explain the flux improvement during ultrafiltration of bentonite suspensions.

Introduction of Intermittency Frequency. The periodic variation in pressure allowed the raw signal to be processed in order to obtain further information about slug-flow hydrodynamics. The spectral analysis of each pressure signal revealed the predominance of a low intermittency frequency whose value depended upon the pipe diameter and the gas and liquid flow rates. An example of this kind of analysis for $D = 6$ mm is presented in Figure 7. The existence of a relatively well-defined peak, particularly in the 6-mm-ID tube, characterized a homogeneous population of Taylor bubbles and liquid slugs. The values of this intermittency frequency, obtained for different Q_G/Q_L ratios, were then plotted vs. the

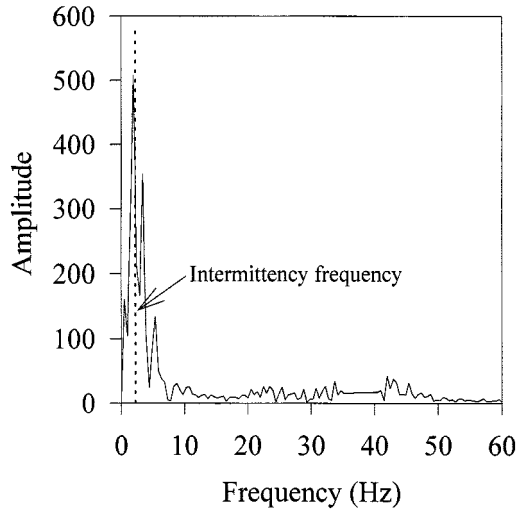

Figure 7. Spectral analysis of a pressure signal for D = 6 mm ($j_L = 1.2\ \mathrm{m \cdot s^{-1}}$ and $j_G = 2\ \mathrm{m \cdot s^{-1}}$).

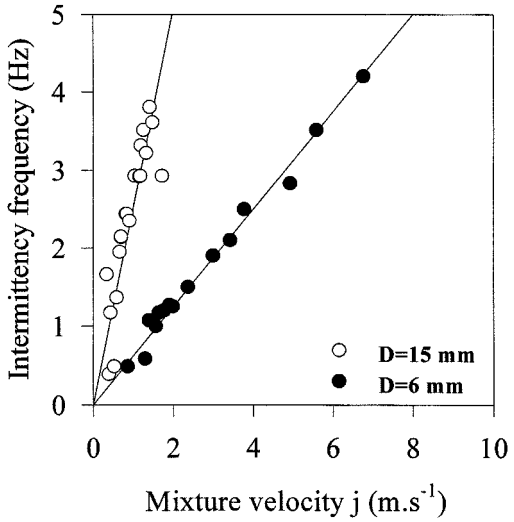

Figure 8. Variation of the flow frequency with the mixture velocity for the two pipe diameters.

corresponding mixture velocity. The frequency was shown to vary linearly with it in the range 0.2–4 Hz (Figure 8). As reported by Fabre and Liné (1992), the mechanism of aeration at the bubble tail should correspond to swarms of bubbles formed in the mixing region and cyclically detached from the mixing vortex, the frequency of these pulses increasing with the velocity of the flow. This phenomenon could thus explain the variation of the frequency with the mixture velocity. The relations obtained depended upon the membrane diameter, and the intermittency was all the more pronounced for the larger diameter. For example, for a mixture velocity equal to 1 $\mathrm{m \cdot s^{-1}}$, the frequency reached 2.4 Hz for $D = 15$ mm, whereas it was only 0.6 Hz for $D = 6$ mm. This possibility of modifying the intermittency characteristics can be very valuable in terms of improving filtration performances. In fact, knowing the nature of the fouling layer, it will be possible to adapt the pressure fluctuation kinetics to the fouling-layer formation kinetics by a suitable choice of experimental conditions, especially the membrane diameter and/or the injected flow rates. This opportunity to limit the particle deposit by time-scale considerations and selection of the most appropriate frequencies has been previously studied by Jaffrin et al. (1995) in bovine blood filtration. The use of this kind of unsteadiness involves, however, the reduction of physicochemical interactions between the membrane and the suspension in order to deal only with an exclusively mechanical problem.

Void-fraction measurements: Application to slug-flow characteristics

The purpose of the present investigation was to characterize the slug-flow behavior in the two tubular geometries by estimating the average void fractions, the lengths, and the velocities of the Taylor bubbles and liquid slugs. Tools for quantitative identification of such an unsteady flow have already been presented. The results of these measurements were then used as a data bank in order to check the extrapolation of the phenomenological model developed by Fabre and Liné (1996), initially for large pipelines and to calculate

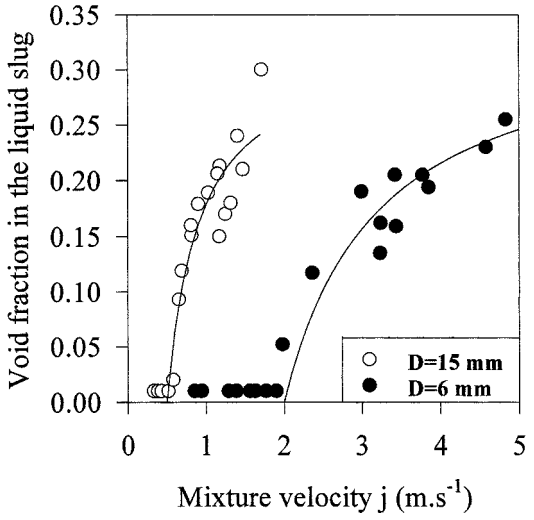

Figure 9. Variation of the void fraction within the liquid slug for the two pipe diameters.

some further data that could not be easily measured by direct experiments (''falling'' liquid-film velocity, wall shear stress, etc.).

Variation in Void Fractions and Lengths. The measured values of the average void fraction in the liquid slugs are shown in Figure 9. Two major effects of diameter could be observed from these measurements. First, there was a lower threshold velocity below which practically no bubbles were present in the slug and this was shown to be dependent on pipe diameter. The limiting velocity was 0.5 $m \cdot s^{-1}$ for $D = 15$ mm, whereas it reached 2 $m \cdot s^{-1}$ for $D = 6$ mm. Second, for the same mixture velocity, liquid slugs in a 6-mm-diameter pipe were always less aerated than in a 15-mm-diameter pipe. This faster increase in void fraction with the mixture velocity for larger diameter pipes was previously observed by Andreussi and Bendiksen (1989) in horizontal gas/liquid flows for different pipe diameters and inclinations. These two effects showed the strong influence of pipe diameter on slug-flow hydrodynamics, especially on the secondary flows generated in the wake of the long bubbles. In the experimental range tested, the mean void fraction within the liquid slug tended to level off at a value of 25% (Figure 9), while the void fraction in the Taylor bubble was, as expected, close to 90% whatever the tube diameter, provided that the bubble was long enough.

In the whole range of mixture velocities considered in this study, the mean slug length for a 15-mm-diameter tube appeared to be practically independent of gas and liquid flow rates and reached a constant value of $13D$, which was in agreement with the conclusions of Fabre and Liné (1992). The slug length stayed constant as it traveled along the tube because liquid was shed from the back of the slug at the same rate as liquid was picked up at the front. On the other hand, the length of long bubbles L_B was a linear function of the Q_G/Q_L ratio, and in the experimental range tested ($40\% < Q_G/Q_L < 200\%$), the aspect ratio L_B/D was between 3 and 15.

For a 6-mm-diameter tube and a wider range of mixture velocities with Q_G/Q_L values high enough, the length of slugs was not constant and varied in the range $75D-150D$ in agreement with visual observations. As for $D = 15$ mm, the length of long bubbles was also a linear function of the Q_G/Q_L ratio, and in the same experimental range, the aspect ratio varied from 40 to 140. For high Q_G/Q_L ratios, it should be noticed that the bubble length was slightly underestimated compared to direct observations. These high values of bubble length could be explained by assuming that the bubble volume was determined by conditions independent of the tube and that they were rather directly related to the geometry of the pipe located just upstream the 6-mm-ID tube (larger diameter). The condition of isovolume for bubbles with the same Q_G/Q_L ratio (in a first approximation, assumption of low exchanges between the bubbles and the slugs) caused an increase in the corresponding length when entering a section of lower diameter. In fact, more precisely, the product $L_B D^2$ was constant, which means that the length of the bubbles should be 6.25 larger in the 6-mm tube than in the 15-mm one. This led to an aspect ratio theoretically 15.6 higher in the smaller tube, and this value was of the same order of magnitude as the difference experimentally observed. This result pointed up the great influence not only of the upstream hydraulic characteristics but also of the injection mode (relative position of gas and liquid supplies) on the two-phase flow structure, especially in narrow tubes.

Bubble Velocity. Following the correlation of Nicklin et al. (1962), it was possible to represent in a 15-mm-diameter pipe the velocity of long bubbles as the sum of two terms: $V = C_0 j + V_\infty$, where j is the mixture velocity, V_∞ is the bubble velocity in a fluid at rest at infinity, and C_0 is a dimensionless coefficient that may remain constant over a certain range of mixture velocities and fluid properties (Figure 10). From the preceding equation, the bubble velocity could be interpreted as the result of the combination of transport by the mean flow and the driving force. In our study, the Reynolds number, which is related to the liquid phase and is defined as $Re_L = (\rho_L j D/\mu_L)$ (μ_L is the viscosity of the liquid phase (Pa·s) and ρ_L is the density of the liquid phase ($kg \cdot m^{-3}$)), was in the range 8,000–22,500. In these conditions (turbulent flow,

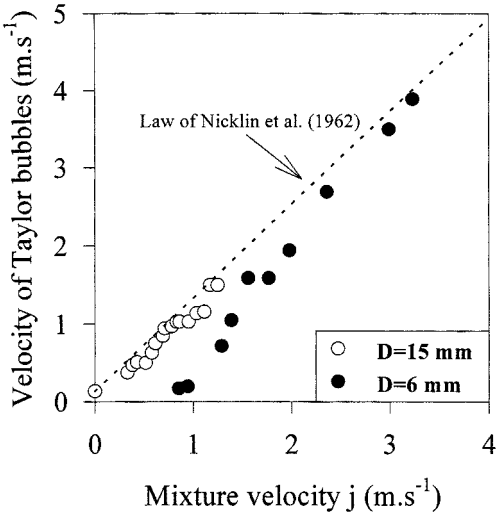

Figure 10. Variation of Taylor bubbles velocity with the mixture velocity for the two pipe diameters.

upward motion) Fréchou (1986) found a C_0 value close to 1.1–1.2 and a V_∞ value of $0.35\sqrt{gD}$ (g is the gravitational acceleration ($m \cdot s^{-2}$)) in a 50-mm-ID tube. These values were experimentally verified in the present investigation for $D = 15$ mm. However, the coefficient C_0 was slightly lower ($C_0 = 1.02$) due to a smaller diameter or a lack of accuracy attributable to too short a distance between the probes, especially for high mixture velocities. The case of the 6-mm-ID tube was quite different. Below a critical value of 0.82 $m \cdot s^{-1}$ for the mixture velocity, the bubbles were motionless, and up to 2 $m \cdot s^{-1}$ their velocity was lower than the mixture velocity (Figure 10). This phenomenon occurred because, under these experimental conditions, the gravity and inertia forces became quite negligible compared to the surface-tension force. Above this threshold, the experimental values fitted the correlation of Nicklin et al. (1962), although at a slightly higher C_0 value ($C_0 = 1.5$). In this range, it should be noticed that the variation in the R_{GD} void fraction had the same evolution as the one observed for $D = 15$ mm (Figure 9). For nearly the same bubble velocity in 15- and 6-mm-ID tubes, and because the slug-flow frequency was also defined as the ratio between the bubble velocity and the cell length (sum of the bubble and slug lengths), the higher frequencies observed for $D = 15$ mm could be explained by lower slug and bubble lengths, as described in the previous section.

In conclusion, by using a relatively simple technique, a substantial amount of information regarding the hydrodynamics of slug flow was obtained. Comparison of quantitative hydrodynamic parameters, like the void fraction within the liquid slug and the Taylor bubble velocity, showed for the same mixture velocities large differences according to the pipe diameter, due to different major mechanisms. These measured values represented a useful database for the phenomenological model developed by Fabre and Liné (1996) in order to understand how slug-flow hydrodynamics acted on filtration flux enhancement.

Modeling of two-phase slug flow: Application to cross-flow filtration

Principle of Modeling. In this part, we briefly present the main results of the model of Fabre and Liné (1996) in order to understand how, allowing for certain modifications due to different pipe geometries and different flow structures, it could be applied in the present investigation.

The complexity of slug flow arose from its particular structure, which was periodic in neither space nor in time. Modeling thus required a detailed analysis, taking into account the intermittent behavior. By reducing intermittency to periodicity, the actual complex flow structure was simplified to an equivalent cell consisting of a long bubble, which was approximated to a cylindrical capsule, and a liquid slug, which was considered as a homogeneous bubbly flow. In the "unit cell model" developed by Fernandes et al. (1983) for vertical slug flow, the main assumption was to describe the flow as a sequence of cells periodic in both space and time.

Recently a formalism has been developed for the hydrodynamic phenomena to be statistically averaged over each flow pattern that constituted the slug flow, namely, the separated and the dispersed flow regions. The method led to the prediction of the dependent variables within each flow pattern and of the characteristics of the intermittency from a "statistical cellular model" based on conditioned averaging of conservation equations. The model developed by Fabre and Liné (1996) for vertical oil pipes was based on the introduction of a characteristic function of intermittency $\chi(x,t)$, which was equal to 1 if certain flow conditions were satisfied at (x,t), and 0 otherwise. It was arbitrarily assigned to 1 for separated flow. By weighting a cross-section of averaged balance equations of each phase by the intermittency function, one obtained the instantaneous balance equations. These were then written in a statistical average form to get averaged expressions, for each phase (gas/liquid) in each flow pattern (dispersed flow D/separated flow S).

In the frame moving at the velocity V of the cells, the unsteady behavior of slug flow was transformed into a steady one. This property constituted the first assumption of the model. The second one was the assumption that the flow was fully developed in each part of the cell. As a consequence, the cross-sectional mean fraction and velocity of each phase did not depend on the longitudinal coordinate inside the Taylor bubbles and liquid slugs. Under these two assumptions, the equations of mass and momentum took a simplified form whose resolution led to void fractions and velocities of each phase over each flow pattern.

Before presenting the simplified equations, we recall here that the model has already been developed in an earlier analysis. For a complete overview of its different parts, and especially the initial form of the balance equations, see the article by Fabre and Liné (1996).

Balance Equations in the Frame Moving at Velocity V. If φ_k represented the volumetric flux of phase-k ($k = L, G$) entering the long bubble region and shed from the liquid slug, one could introduce the definitions of the mean velocities U_k, U_{kS}, U_{kD} of phase k through the following equations:

$$\varphi_k = R_{kS}(V - U_{kS}) = R_{kD}(V - U_{kD}) = R_k(V - U_k) = R_k V - j_k,$$

where R_k, R_{kS}, R_{kD} represented the space-average of phase fractions over the cell, V the velocity of Taylor bubbles, and j_k the superficial velocity of phase k. The resolution of the cross-sectional average of the momentum equation for phase k in the moving frame led over each part of the cell to:

$$R_{kS}\frac{dP_s}{dx} = T_{kWS} + T_{kIS} - \rho_k R_{kS} g \sin\theta$$

(here $\sin\theta = 1$ since $\theta = 90°$, θ: inclination)

$$R_{kD}\frac{dP_D}{dx} = T_{kWD} + T_{kID} - \rho_k R_{kD} g.$$

In these equations, P is the mean pressure over the cross-sectional area of phase k and ρ_k the density of the phase k. The wall and interfacial frictions T_{kW} and T_{kI} over each part of the cell are related to the wetted perimeter (S_{kW} and S_{kI}) and the x-component of the stress exerted upon the phase k by the wall or the interface by

$$T_{kW(I)} = \frac{\tau_{kW(I)} S_{kW(I)}}{A},$$

where A is the cross section of the tube.

The network of equations available to solve the problem was the following:

In the first part of the cell (separated flow)
Mass balance:

$$\varphi_G = R_{GS}(V - U_{GS}) \tag{1}$$

$$\varphi_L = R_{LS}(V - U_{LS}). \tag{2}$$

Momentum balance:

$$-R_{GS}\frac{dP_S}{dx} = -T_{GIS} + \rho_G R_{GS} g \tag{3}$$

(the gas phase is not in contact with the wall)

$$-R_{LS}\frac{dP_S}{dx} = T_{GIS} - T_{LWS} + \rho_L R_{LS} g \tag{4}$$

$$\left(\text{with the jump condition: } \sum_{k=L,G} T_{kIS(D)} = 0\right).$$

$$\text{Algebraic relation: } R_{GS} + R_{LS} = 1. \tag{5}$$

In the second part of the cell (dispersed flow)
Mass balance:

$$\varphi_G = R_{GD}(V - U_{GD}) \tag{6}$$

$$\varphi_L = R_{LD}(V - U_{LD}). \tag{7}$$

Momentum balance:

$$-R_{GD}\frac{dP_D}{dx} = -T_{GID} + \rho_G R_{GD} g \tag{8}$$

$$-R_{LD}\frac{dP_D}{dx} = T_{GID} - T_{LWD} + \rho_L R_{LD} g. \tag{9}$$

$$\text{Algebraic relation: } R_{GD} + R_{LD} = 1. \tag{10}$$

By adding the two momentum equations, one obtains:

$$-\frac{dP_D}{dx} = -T_{LWD} + g(\rho_G R_{GD} + \rho_L R_{LD}). \tag{8'}$$

To restore the subsequent missing information, our choice was to use the drift flux model for the bubbly region:

$$U_{GD} = C_1 j + V_B(1 - C_m R_{GD})(1 - R_{GD}), \tag{9'}$$

in which C_1 accounts for the velocity and gas fraction distribution ($C_1 \approx 1$); C_m is the entrained mass coefficient ($C_m \approx 0.5$); and V_B is the rise velocity of bubble in still liquid (Gadoin, 1993).

Further information over the entire cell was then given:

- The mean phase fraction could be expressed vs. the phase fractions in each part of the cell through

$$R_G = \beta R_{GS} + (1 - \beta) R_{GD} \quad \text{(idem for the liquid)}. \tag{11}$$

- The mean pressure gradient over the cell resulted from the mean pressure gradient over each part of the cell weighted by their rate of occurrence:

$$\frac{dP}{dx} = \beta\frac{dP_S}{dx} + (1 - \beta)\frac{dP_D}{dx}. \tag{12}$$

- The other relations were:

$$\varphi_G = R_G V - j_G \tag{13}$$

$$\varphi_L = R_L V - j_L \tag{14}$$

$$R_G + R_L = 1. \tag{15}$$

The unknowns were as follows:

$$R_G,\ R_L,\ \frac{dP}{dx},\ \varphi_G,\ \varphi_L,$$
$$R_{LS},\ R_{GS},\ \frac{dP_s}{dx},\ U_{GS},\ U_{LS},$$
$$R_{LD},\ R_{GD},\ \frac{dP_D}{dx},\ U_{GD},\ U_{LD},\ V,\ V_B,\ \beta,$$
$$\tau_{GIS},\ \tau_{LWS},\ \tau_{LWD},\ S_{GIS},\ S_{LWS},\ S_{LWD}.$$

which total 24.

The equation network (15 independent equations) was thus not sufficient to provide a closed-form solution and nine further equations, noted from (a) to (i) in the following subsection, had to be added.

Closure Laws. In our case, the first empirical closure law was the velocity of the Taylor bubbles:

$$V \tag{a}$$

The rise velocity of small bubbles in still liquid (V_B) was, in a first approximation, considered to be independent of bubble size, depending only on the fluid properties (Fernandes et al., 1983). It was thus expressed as follows:

$$V_B = 1.53\left(\frac{\sigma_L g \Delta\rho}{\rho_L^2}\right), \tag{b}$$

with $\Delta\rho = \rho_L - \rho_G$ and σ_L: surface tension of the liquid (kg·s^{-2}) (Harmathy, 1960).

The wetted perimeters were determined thanks to geometrical relations taking into account the pipe characteristics:

$$S_{LWS} = \pi D \tag{c}$$

$$S_{LWD} = \pi D \tag{d}$$

$$S_{GIS} = \pi(D - 2e) \quad \text{with} \quad e = \frac{D}{2}\left(1 - \sqrt{R_{GS}}\right). \tag{e}$$

The shear stress at both wall (τ_{LWS}, τ_{LWD}) and interface (τ_{GIS}) were expressed by single-phase relationships:

$$|\tau_{LWS}| = f_{LWS}\rho_L\frac{U_{LS}^2}{2} \tag{f}$$

$$|\tau_{LWD}| = f_{LWD}\,\rho_L \frac{U_{LD}^2}{2} \qquad \text{(g)}$$

$$|\tau_{GIS}| = f_{GIS}\,\rho_G \frac{(U_{GS} - U_{LS})^2}{2}, \qquad \text{(h)}$$

in which the friction factors f_{LWS}, f_{LWD}, f_{GIS} were calculated by single-phase correlations: for laminar flow, Poiseuille relation, and for turbulent flow and both smooth and rough pipes, Colebrook law (Gadoin, 1993). For example, for f_{LWS}:

$$f_{LWS} = \frac{16}{Re_{LS}}$$

$$\frac{1}{2\sqrt{f_{LWS}}} = 1{,}74 - 2\log\left(\frac{2k_W}{Dh_{LS}} + \frac{9{,}35}{Re_{LS}\sqrt{f_{LWS}}}\right),$$

where k_W, Dh_{LS}, Re_{LS} are, respectively, the wall roughness, the hydraulic diameter, and the Reynolds number

$$\left(Re_{LS} = \frac{Dh_{LS}U_{LS}\,\rho_L}{\mu_L} \quad \text{with} \quad Dh_{LS} = \frac{4A}{S_{LWS}}\right).$$

Instead of choosing β as a datum of the closure problem, we decided to consider the evolution of the average void fraction in liquid slugs R_{GD}, since this parameter could easily be accessible by conductance measurements. Its variation vs. the mixture velocity has basically the same trend in horizontal and vertical pipes (Fabre and Liné, 1996). Therefore it has been suggested that the same physical processes took place (especially mechanism of entrainment at the bubble tail) and the same modeling could be used whatever the pipe slope. We thus adapted the model proposed by Andreussi and Bendiksen (1989) and we postulated that the void fraction could be estimated as follows:

$$R_{GD} = \frac{j - j_f}{aj + j_0}. \qquad \text{(i)}$$

In this equation, whose form is slightly different from the original one, the critical mixture velocity j_f is experimentally determined (velocity below which no bubbles are present in the slug), whereas the velocity scale j_0 and the coefficient a are chosen for each pipe geometry for the best fit with experimental data. The resulting values for j_f, a and j_0 are, respectively, 0.5 $\mathrm{m\cdot s^{-1}}$, 3.1, and -0.3 $\mathrm{m\cdot s^{-1}}$ for $D = 15$ mm, and 2 $\mathrm{m\cdot s^{-1}}$, 2.9, and -2.3 $\mathrm{m\cdot s^{-1}}$ for $D = 6$ mm. Thanks to all these closure laws, the problem could be easily solved.

Results of Modeling: Comparison of Modeling with Experiment. In order to validate the extrapolation of the model of Fabre and Liné (1996) in 6- and 15-mm-diameter tubes, the experimental and theoretical values for R_G and β were compared. β was experimentally estimated as the ratio between the length of the Taylor bubble and the length of the cell unit. The theoretical value of β was defined as follows:

$$\beta = \frac{R_G - R_{GD}}{R_{GS} - R_{GD}}.$$

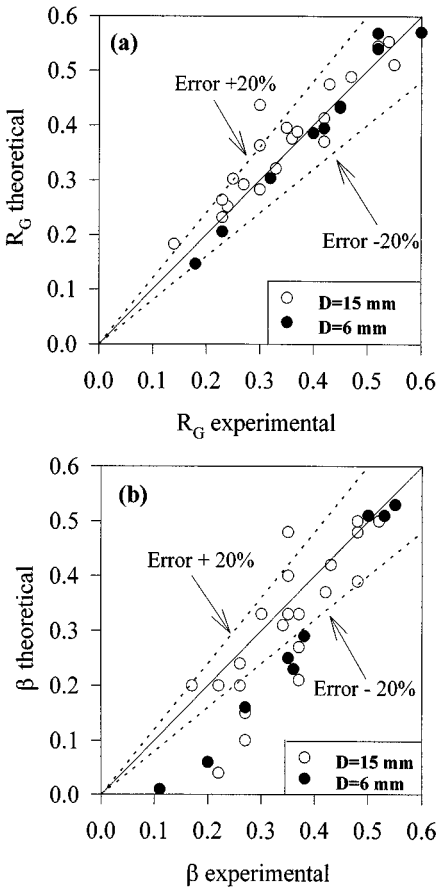

Figure 11. Comparison of theoretical and measured values for the two pipe diameters.

(a) Global void fraction R_G; (b) rate of intermittency β.

For the R_G estimation, the same relation was applied with alternatively experimental and theoretical values of β, R_{GS}, and R_{GD}. For $D = 6$ mm, the reported values corresponded to a bubble velocity higher than the mixture velocity.

In all cases, for 15-mm and 6-mm inner diameters, the agreement was quite satisfactory concerning the R_G calculations. Average relative error in predicting R_G was less than 20% (Figures 11a and 11b). Nevertheless, although a good prediction for R_G was obtained, the agreement for the rate of intermittency in both pipes was found to be less satisfactory, especially for small values that corresponded to Q_G/Q_L ratios lower than 50% (Figure 11b). The discrepancy was explained by an overestimation of the void fraction R_{GS}, and several hypothesis could be formulated, the poor prediction of the hydrodynamics in the liquid film being one of them.

Quantification of Slug-Flow Hydrodynamics. To characterize the slug-flow hydrodynamics in 6- and 15-mm-diameter tubes, the wall shear stresses in liquid slugs (τ_{WD} instead of τ_{LWD}) and in the liquid film around the Taylor bubbles (τ_{WS} instead of τ_{LWS}) were calculated for different air and liquid velocities. Examples of this kind of calculation are shown in Tables 1 ($D = 15$ mm) and 2 ($D = 6$ mm). The velocities of the liquid film (U_{LS}) were also listed to verify the "falling film" assumption.

Table 1. Modeling for $D = 15$ mm for Different Gas and Liquid Superficial Velocities

j_L (m·s^{-1})	j_G (m·s^{-1})	j (m·s^{-1})	τ_{WD} (Pa)	τ_{WS} (Pa)	U_{LS} (m·s^{-1})
0.24	0.09	0.33	−0.53	4.27	−0.73
0.22	0.16	0.38	−0.68	4.17	−0.71
0.22	0.21	0.43	−0.82	4.08	−0.70
0.23	0.29	0.52	−1.13	3.92	−0.67
0.23	0.35	0.58	−1.32	3.87	−0.66
0.45	0.21	0.66	−1.57	3.78	−0.65
0.45	0.37	0.82	−2.18	3.55	−0.60
0.44	0.46	0.90	−2.55	3.45	−0.58
0.45	0.58	1.03	−3.15	3.30	−0.54
0.45	0.73	1.18	−3.90	3.15	−0.50

Note: Wall shear stress in the liquid slug τ_{WD} and in the liquid film around the Taylor bubble τ_{WS}, film velocity U_{LS}.

From these calculations, we concluded that a gas/liquid slug flow consisted of a succession of positive raised shear stresses and negative shear stresses with high absolute values linked to the mixture velocity. This reversal, related to the operating parameters through the flow frequency, was involved in the control of the cake characteristics. We could also verify that, for each experimental condition, the annular liquid film around the Taylor bubble flowed downward, in the opposite direction to the main flow. The absolute value of the film velocity was higher in a 15-mm-ID pipe even for lower mixture velocities. This could explain the formation of more aerated slugs for the same velocity, since the bubble production rate at the long bubble tail is proportional to the film flow rate, provided that the flow rate exceeds a certain lower limit (Andreussi and Bendiksen, 1989). However, the part of the gas that returned to the Taylor bubble by the vortex motion remained to be quantified for each pipe geometry.

Correlation Between the Flux Enhancement and the Slug-Flow Hydrodynamics. In this subsection, we try to correlate the external conditions (gas and liquid flow rates) to the local hydrodynamic parameters, such as the intermittency rate or the wall shear stress, in a 15-mm-diameter tube by introducing a variable linked only to the gas-phase influence. To this end, the theoretical intermittency rate was connected to the gas and liquid flow rates (Figure 12). We should note that, for some flow conditions with a poor model prediction, the experimental values were preferred. The resulting linear relation clearly indicated that the rate of intermittency was directly dependent upon the operating conditions, that is, the gas and liquid flow rates. The slope of the curve accounted for the structure and the unsteady characteristics of slug flow.

Table 2. Modeling for $D = 6$ mm for Different Gas and Liquid Superficial Velocities

j_L (m·s^{-1})	j_G (m·s^{-1})	j (m·s^{-1})	τ_{WD} (Pa)	τ_{WS} (Pa)	U_{LS} (m·s^{-1})
2.75	0.49	3.24	−33.5	1.29	−0.09
2.70	0.74	3.44	−36.5	1.44	−0.12
2.59	1.26	3.85	−43.0	1.65	−0.15
2.64	1.95	4.59	−57.0	1.86	−0.20

Note: Wall shear stress in the liquid τ_{WD} and in the liquid film around the Taylor bubble τ_{WS}, film velocity U_{LS}.

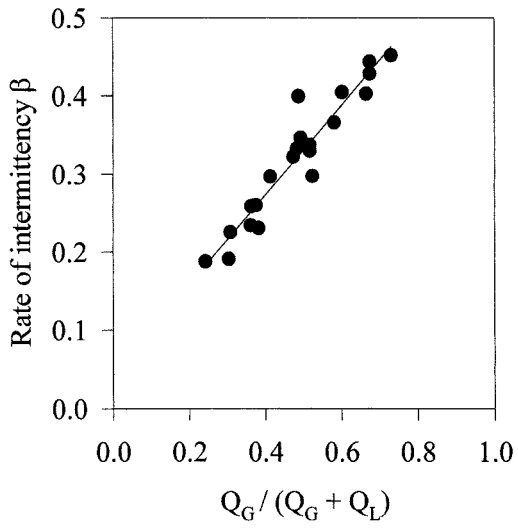

Figure 12. Relation between the rate of intermittency and the gas and liquid flow rates for $D = 15$ mm.

The wall shear stress variation vs. the theoretical intermittency rate was then plotted in Figure 13. The shear stress values in the Taylor bubble remained almost the same, due to a nearly constant velocity of the "falling" liquid film. On the other hand, the increase in the absolute value of shear stress in the liquid slug could be explained by higher mixture velocities. By extrapolating the relations to $\beta = 0$ for each liquid flow rate, the resulting flow pattern should correspond to a bubbly flow. However, in our case, since the gas flow rates were low enough compared to liquid ones, we could treat it as a single-phase flow at j_L velocity. This explained that for $\beta = 0$, each wall shear stress corresponded to the value calculated according to single-phase correlations as-

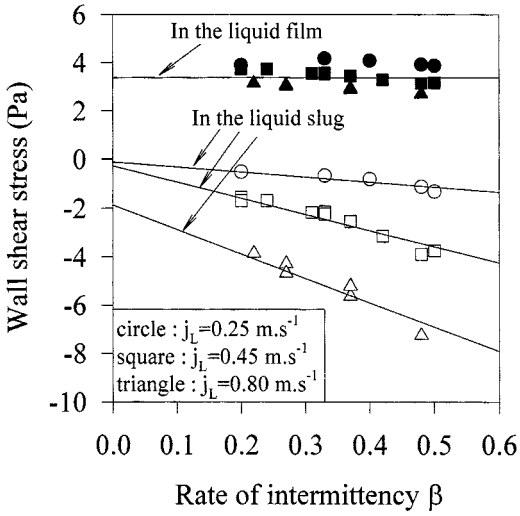

Figure 13. Variation of the wall shear stress vs. the rate of intermittency for $D = 15$ mm in the liquid slug and in the film around the Taylor bubble.

suming a smooth pipe (see below for the calculations). It could be concluded from these observations that in the liquid slug the theoretical wall shear was made up to of two contributions: the influence of the gas phase and that of the associated liquid flow.

Taking into account the unsteady slug-flow characteristics, the total wall shear stress, τ_{WT} was then introduced and defined as follows: $\tau_{WT} = \beta|\tau_{WS}| + (1-\beta)|\tau_{WD}|$. The choice of absolute values for τ_{WS} and τ_{WD} could be explained by an erosion of particle deposit caused mainly by the shear-stress value and not by its sign. As previously mentioned, the periodic reversal was rather important in the destabilization of the formed fouling layer. Another variable τ_W^*, which was chosen as a specific parameter, was defined to take into account only the influence of the gas phase. It was therefore calculated as follows: $\tau_W^* = \tau_{WT} - |\tau_{WSP}|$, which agrees with the previous observations related to the shear-stress variation in the liquid slug. τ_{WSP} corresponded to the single-phase flow at j_L velocity and was calculated as follows: $|\tau_{WSP}| = \rho_L(f_{SP}/2)\, j_L^2$ with a friction factor f_{SP} of $6.25 \cdot 10^{-3}$ (smooth pipe). The τ_{WSP} values were -0.2, -0.6, and -2.0 Pa for J_L values close to 0.25, 0.45, and 0.80 $m \cdot s^{-1}$ respectively. We should recall here that the choice of τ_{WSP} for processing our data could also be explained by the experimental procedure used during steady (no air addition) and unsteady (air addition) filtration assays, which consisted of testing the influence of gas sparging with the same liquid velocity (Mercier et al., 1997).

The next step consisted of correlating the shear stress τ_W^* with the intermittency rate on the following assumption: for $\beta = 0$, the τ_W^* value was equal to zero. The resulting relations were linear and enabled τ_W^* to be calculated from the knowledge of the operating conditions (liquid and gas flow rates) through the estimation of the rate of intermittency. Thanks to these correlations, it was then possible to represent the variation of the parameter K_j vs. the τ_W^* shear stress for the same experimental conditions (Figure 14). It must be seen that these additional shear stresses, though fairly small in their absolute values (1–3 Pa), were significant compared to the corresponding single-phase shear stresses. The reported values of K_j corresponded to ultrafiltration assays (S.C.T. mineral tubular membranes) of suspensions of bentonite and biological yeasts (Mercier et al., 1997). We should recall here that K_j was defined as the ratio between the flux as obtained after 180 min of filtration in unsteady and steady conditions. The close relation between K_j and τ_W^* satisfactorily showed that the flux improvement, experimentally obtained under these filtration conditions, was partly achieved thanks to the enhancement of the wall shear stress, induced by air injection inside the membrane unit. For yeasts at low concentrations (1 $g \cdot L^{-1}$), the external fouling due to the particle deposit did not predominate compared to other limiting phenomena (internal fouling like molecular adsorption or pore plugging). As a consequence, the efficiency of the two-phase flow technique was not maximal, since the main objective of unsteady flow techniques was to reduce the thickness of the fouling layer formed at the membrane surface. This could explain the increasing discrepancy observed for yeasts at 1 $g \cdot L^{-1}$. For the 6-mm-ID membrane, the same procedure could not be applied because of the lack of significant experiments with suitable operating conditions. However, the variation of the wall shear stress in the Taylor bubble and in the liquid slug vs. the rate of intermittency, observed for $D = 15$ mm, was confirmed here.

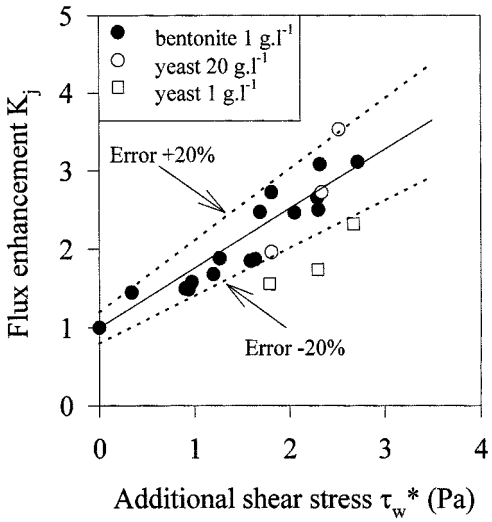

Figure 14. Correlation between the flux enhancement (K_j) and the wall shear stress τ_W^* for $D = 15$ mm.

Discussion

By using a conductance probe technique that allowed precise and reproductible measurements of void fractions, it was possible to characterize the slug-flow hydrodynamics and to predict its variation with respect to the modification of the external operating conditions (pipe diameters, liquid and gas flow rates). This study focused in particular on the structural differences in both geometries investigated ($D = 6$ and 15 mm), due to surface-tension forces that could no longer be neglected compared to convection forces. In some flow rate ranges and fluid properties, the hydrodynamic behavior was thus strictly distinct in terms of void fraction within the liquid slugs or velocity of long bubbles. In our system, other characteristics such as cell length or rate of intermittency were also different. As a consequence, the phenomenological approach used in the model of Fabre and Liné (1996) in large diameters was not directly extrapolable, as it stood, for narrow tubes in this range of flow conditions. Another point to deal with arose from the comparison of the theoretical film thickness (e) and the experimental one, as deduced from high-speed photographic observations or the interpretation of conductance signals [$e = (D/2)(1 - \sqrt{R_{GS}})$]. We should note that both experiments gave the same results. Then the comparison with a 15-mm-ID tube showed that the model underestimated the film thickness, since the mean theoretical and experimental values over the whole range of experimental conditions were 0.5 and 0.9 mm, respectively. As previously mentioned, the discrepancy was attributable to an overestimation of the calculated void fraction in the Taylor bubble. This modeling weakness, particularly important for bubbles a few diameters long, was explained by the fully developed flow assumption being no longer satisfied. In the case of the forma-

tion of smaller bubbles, it is therefore required that the model basis be modified in order to take their hydrodynamics into account, especially in the front curvature region. For narrow tubes, it will be also necessary to adapt the existing relations in order to take the influence of surface tension on slug flow hydrodynamics into account. In terms of closure laws, the empirical correlations established for the bubble velocity and the void fraction in the slug in our geometries will have to be validated by more theoretical considerations. The influence of the increasing pressure variations in the bubble wake will also have to be understood and modeled. From another point of view, direct experiments based, for example, on the measurement of the wall shear stress will be useful to confirm the model predictions. To this end, several methods may be investigated, for example, electrochemical techniques.

By studying more accurately the influence of pipe diameter on slug-flow structure, the empirical introduction of a new reference scale defined as the product of the mixture velocity and the diameter to the power of 1.5 ($jD^{1.5}$) enabled all the experimental points concerning the intermittency frequency or the void fraction R_{GD} to be collected on the same curve for the two geometries (results not shown). This parameter, which was common to both series of independent experiments, could surely account for the role of diameter on slug-flow hydrodynamics. However, the theoretical explanation for such a parameter remains to be found, since it was not related to nondimensional numbers usually considered in two-phase flow analysis (Froude, Eötvos, or Reynolds number).

In spite of the actual modeling weakness on some hydrodynamic information, the main results of the present analysis could be applied without doubt to the understanding of fouling limitation by slug-flow hydrodynamics. The common efficiency experimentally observed for ultrafiltration assays in the two kinds of membranes ($K_j = 3$) (Mercier et al., 1997, 1998) revealed that hydrodynamic phenomena linked to the fouling limitation were of the same kind, although the initial hydrodynamic characteristics are different. It was difficult to dissociate them since they were all involved to different degrees in the process efficiency, according to the membrane geometry. The present investigation allowed a more accurate characterization not only of their nature but also their mechanical action. The increase in wall shear stress compared to single-phase flow acted on the erosion of the particle deposit by inducing a periodic sweeping effect. This mechanism of erosion could not explain the overall flux enhancement by itself, since the ultrafiltration flux with gas sparging always remained higher than that with no gas injection, the corresponding liquid flow rate being adjusted to impose the same total wall shear stress inside the membrane. For example, from the interpretation of some filtration results obtained with the bentonite suspension (Mercier et al., 1997), the flux enhancement with the same total wall shear stress was about 55% ($K_j = 1.55$). Therefore, other phenomena associated with the intermittent succession of Taylor bubbles and liquid slugs were at play in the deposit destabilization and subsequent improvement in mixing and mass transfer: reversal of the wall shear stress, pressure fluctuations, and turbulence enhancement in the long bubble wake. The actual correlation between the flux improvement and the raised shear stress will have to be refined by the inclusion of all these effects with the important factors linked to the geometry considered.

The improved knowledge of two-phase flow unsteadiness also enabled the main characteristics to be identified, which could be of interest in cross-flow filtration compared to other existing techniques. First, the instantaneous pressure decreases allowed a constant mean transmembrane pressure to be maintained throughout the filtration experiment, whereas in pulsing or oscillatory flows, the pressure profile was often characterized by compression and decompression phases with the same average duration (Gupta et al., 1992). In this two-phase flow technique, however, the frequency could not be directly controlled, as it was determined by the succession rates of bubbles and slugs. The control was in fact achieved through the modification of experimental conditions (injection system, membrane diameter, liquid and gas flow rates). In addition, the selection of the most appropriate frequency according to the kinetics of deposit formation could help to optimize the process efficiency. Second, the pressure and velocity fluctuations were entirely uncoupled since, at a given point in the flow, the value and sign of velocity depended upon the residence time of the long bubbles and liquid slugs, whereas the pressure always remained the same except for momentary decreases due to the bubble wake. This possibility of uncoupling could be particularly important in terms of reducing particle fouling, as most unsteady techniques were actually limited by a strong dependency between operating parameters (Doubrovine, 1992).

Conclusions

The present work reports on the characterization of slug-flow hydrodynamics in two kinds of membrane diameters in order to identify the main phenomena that are involved in the limitation of particle fouling. By using a relatively simple and reliable method, a substantial amount of information regarding the flow structure was obtained. Noticeable differences were observed for the most narrow tubes ($D = 6$ mm), thus proving that, in some experimental range, convective forces no longer predominated over surface-tension forces.

In a larger membrane diameter ($D = 15$ mm), the prior determination of quantitative hydrodynamic parameters of slug flow allowed some further data (wall shear stress, ''falling'' liquid-film velocity, film thickness) to be calculated thanks to modeling. The results showed that the flux improvement was partly due to the increase in the wall shear stress, induced by continuous gas sparging inside the tubular filtration module. Other hydrodynamic phenomena linked to the intermittent succession of Taylor bubbles and liquid slugs were also involved in the particle-deposit limitation through an enhancement of mass transfer: reversal of the wall shear stress, pressure variations in the bubble wake, with a higher level of local turbulence. It can be concluded that the quantitative characterization of slug flow offered some useful information regarding the interactions between fouling mechanisms and unsteady hydrodynamics. This work can thus help optimize the hydrodynamic methods for enhancing filtration performances.

From a more theoretical point of view, the modeling presented here constitutes a first tool in understanding the hydrodynamics of slug flow in narrow tubes, but some basic modifications remain to be made and tested. From another point of view, it will be necessary to study the influence of

the injection mode on the flow characteristics (cell length, frequency), in order to complete our knowledge of slug-flow hydrodynamics and to optimize its application during crossflow filtration. Further experimental study of other membrane geometries that combine the filtration and hydrodynamics aspects will also be required to confirm the efficiency of slug flow when applied to industrial-sized membrane systems.

Acknowledgments

The authors wish to thank Christophe Ellero for his technical help. They are also grateful to Catherine Colin and the Interface Group of the Institute of Fluid Mechanics (Toulouse) for helpful discussions about the use of conductivity probes.

Notation

P_D = pressure over the cross-sectional area of phase k in dispersed flow
P_S = pressure over the cross-sectional area of phase k in separated flow
Q_k = volumetric flow rate of phase k
R_k = cross-sectional fraction of phase k over the cell
R_{kD} = cross-sectional fraction of phase k in dispersed flow
R_{kS} = cross-sectional fraction of phase k in separated flow
S_{kID} = wetted perimeter of phase k related to the interface in dispersed flow
S_{kWD} = wetted perimeter of phase k related to the wall in dispersed flow
S_{kIS} = wetted perimeter of phase k related to the interface in separated flow
S_{kWS} = wetted perimeter of phase k related to the wall in separated flow
T_{kID} = interfacial friction of phase k in dispersed flow
T_{kWD} = wall friction of phase k in dispersed flow
T_{kIS} = interfacial friction of phase k in separated flow
T_{kWS} = wall friction of phase k in separated flow
U_k = velocity of phase k over the cell
U_{kD} = velocity of phase k in dispersed flow
U_{kS} = velocity of phase k in separated flow
x = axial coordinate
β = rate of intermittency defined as the ratio between the bubble length and the cell length
μ_k = dynamic viscosity of phase k
σ_k = surface tension of phase k
τ_{kID} = shear stress exerted upon the phase k by the interface in dispersed flow
τ_{kWD} = shear stress exerted upon the phase k by the wall in dispersed flow
τ_{kIS} = shear stress exerted upon the phase k by the interface in separated flow
τ_{kWS} = shear stress exerted upon the phase k by the wall in separated flow
τ_{WSP} = wall shear stress under single-phase flow at j_L velocity
τ_{WT} = total wall shear stress over the cell

Subscripts

D = dispersed flow
S = separated flow

Literature Cited

Andreussi, P., and K. Bendiksen, ''An Investigation of Void Fraction in Liquid Slugs for Horizontal and Inclined Gas-Liquid Pipe Flow,'' *Int. J. Multiphase Flow*, **15**, 937 (1989).

Arroyo, G., and C. Fonade, ''Use of Intermittent Jets to Enhance Flux in Crossflow Filtration,'' *J. Memb. Sci.*, **80**, 117 (1993).

Bellara, S. R., Z. F. Cui, and D. S. Pepper, ''Gas Sparging to Enhance Permeate Flux in Ultrafiltration Using Hollow Fibre Membranes,'' *J. Memb. Sci.*, **121**, 175 (1996).

Bibal, B., Y. Vayssier, G. Goma, and A. Pareilleux, ''High Concentration Cultivation of *Lactococcus cremoris* in a Cell Recycle Reactor,'' *Biotechnol. Bioeng.*, **37**, 746 (1991).

Cabassud, C., S. Laborie, and J. M. Laine, ''How Slug Flow Can Improve Ultrafiltration Flux in Organic Hollow Fibres,'' *J. Memb. Sci.*, **128**, 93 (1997).

Cui, Z. F., and K. I. T. Wright, ''Gas-Liquid Two-Phase Crossflow Ultrafiltration of BSA and Dextran Solutions,'' *J. Memb. Sci.*, **90**, 183 (1994).

Cui, Z. F., and K. I. T. Wright, ''Flux Enhancements with Gas Sparging in Downwards Crossflow Ultrafiltration: Performance and Mechanism,'' *J. Memb. Sci.*, **117**, 109 (1996).

Doubrovine, N., ''Influence d'un Écoulement Instationnaire Intermittent sur les Performances d'un Procédé de Filtration Tangentielle,'' PhD Thesis, Institut National des Sciences Appliquées, Toulouse, France (1992).

Fabre, J., and A. Liné, ''Modeling of Two-Phase Slug Flow,'' *Annu. Rev. Fluid Mech.*, **24**, 21 (1992).

Fabre, J., and A. Liné, *Encyclopedia of Heat and Mass Transfer — Slug Flow Modeling*, G. F. Hewitt, G. L. Shires, and Y. V. Polezhaev, eds. CRC Press, New York (1996).

Fernandes, R. C., R. Semiat, and A. E. Dukler, ''A Hydrodynamic Model for Gas-Liquid Slug Flow in Vertical Tubes,'' *AIChE J.*, **29**, 981 (1983).

Ferras, E., M. Minier, and G. Goma, ''Acetonobutylic Fermentation: Improvement of Performances by Coupling Continuous Fermentation and Ultrafiltration,'' *Biotechnol. Bioeng.*, **28**, 523 (1986).

Finnigan, S. M., and J. A. Howell, ''The Effect of Pulsatile Flow on UF Fluxes in a Baffled Tubular Membrane System,'' *Desalination*, **79**, 181 (1990).

Fréchou, D., ''Etude de L'Écoulement Ascendant à Trois Fluides en Conduite Verticale,'' PhD Thesis, Institut National Polytechnique, Toulouse, France (1986).

Gadoin, E., ''Régime Intermittent Gaz-Liquide en Conduite Horizontale: Écoulements non Établis et Transitoires,'' PhD Thesis, Institut National Polytechnique, Toulouse, France (1993).

Gupta, B. B., P. Blanpain, and M. Y. Jaffrin, ''Permeate Flux Enhancement by Pressure and Flow Pulsations in Microfiltration with Mineral Membranes,'' *J. Membr. Sci.*, **70**, 257 (1992).

Harmathy, T. Z., ''Velocity of Large Drops and Bubbles in Media of Infinite or Restricted Extent,'' *AIChE J.*, **6**, 281 (1960).

Jaffrin, M. Y., L. H. Ding, M. Defossez, and J. M. Laurent, ''Interpretation of Transient Ultrafiltration and Microfiltration of Blood and Protein Solutions,'' *Chem. Eng. Sci.*, **50**, 907 (1995).

Kroner, K. H., V. Nissinen, and H. Ziegler, ''Improved Dynamic Filtration of Microbial Suspensions,'' *Biotechniques*, **5**, 921 (1987).

Lee, C. K., W. G. Chang, and Y. H. Ju, ''Air Slugs Entrapped Crossflow Filtration of Bacterial Suspensions,'' *Biotechnol.*, **41**, 525 (1993).

Léonard, D., M. Mercier-Bonin, N. D. Lindley, and C. Lafforgue, ''A Novel Membrane Bioreactor with Gas/Liquid Two-Phase Flow for High Performance Degradation of Phenol,'' *Biotechnol. Prog.*, **14**, 680 (1998).

Maranges, C., ''Etude de l'Influence d'un Jet Instationnaire Turbulent sur les Performances de la Filtration Tangentielle: Application aux Bioréacteurs à Membranes,'' PhD Thesis, Institut National des Sciences Appliquées, Toulouse, France (1995).

Maranges, C., and C. Fonade, ''Flux Enhancement in Crossflow Filtration Using an Unsteady Jet,'' *J. Memb. Sci.*, **123**, 1 (1997).

Mercier, M., C. Fonade, and C. Lafforgue-Delorme, ''How Slug Flow Can Enhance the Ultrafiltration Flux in Mineral Tubular Membranes,'' *J. Memb. Sci.*, **128**, 103 (1997).

Mercier, M., C. Maranges, C. Fonade, and C. Lafforgue-Delorme, ''Yeast Suspension Filtration: Flux Enhancement Using an Upward Gas/Liquid Slug Flow—Application to Continuous Alcoholic Fermentation with Cell Recycle,'' *Biotechnol. Bioeng.*, **58**, 47 (1998).

Moulin, P., J. C. Rouch, C. Serra, M. J. Clifton, and P. Aptel, ''Mass Transfer Improvement by Secondary Flows: Dean Vortices in Coiled Tubular Membranes,'' *J. Memb. Sci.*, **114**, 235 (1996).

Nicklin, D. J., J. O. Wilkes, and J. F. Davidson, ''Two-Phase Flow in Vertical Tubes,'' *Trans. Inst. Chem. Eng.*, **40**, 61 (1962).

Manuscript received Mar. 23, 1999, and revision received Sept. 14, 1999.